ChemPubSoc Europe

DOI: 10.1002/cbic.201800801

CHEMBIOCHEM Full Papers

Manipulating Active Structure and Function of Cationic Antimicrobial Peptide CM15 with the Polysulfonated Drug Suramin: A Step Closer to in Vivo Complexity

Mayra Quemé-Peña,[a] Tünde Juhász,*[a] Judith Mihály,[a] Imola Cs. Szigyártó,[a] Kata Horváti,[b] Szilvia Bősze,[b] Judit Henczkó,[c] Bernadett Pályi,[c] Csaba Németh,[a] Zoltán Varga,[a] Ferenc Zsila,[a] and Tamás Beke-Somfai*[a]

Antimicrobial peptides (AMPs) kill bacteria by targeting their membranes through various mechanisms involving peptide assembly, often coupled with disorder-to-order structural transition. However, for several AMPs, similar conformational changes in cases in which small organic compounds of both endogenous and exogenous origin have induced folded peptide conformations have recently been reported. Thus, the function of AMPs and of natural host defence peptides can be significantly affected by the local complex molecular environment in vivo; nonetheless, this area is hardly explored. To address the relevance of such interactions with regard to structure and function, we have tested the effects of the therapeutic drug suramin on the membrane activity and antibacterial efficiency of CM15, a potent hybrid AMP. The results provided insight into a dynamic system in which peptide interaction with lipid bilayers is interfered with by the competitive binding of CM15 to suramin, resulting in an equilibrium dependent on peptide-to-drug ratio and vesicle surface charge. In vitro bacterial tests showed that when CM15·suramin complex formation dominates over membrane binding, antimicrobial activity is abolished. On the basis of this case study, it is proposed that small-molecule secondary structure regulators can modify AMP function and that this should be considered and could potentially be exploited in future development of AMP-based antimicrobial agents.

Introduction

Antibiotic resistance has reached alarming levels and represents one of the biggest current global threats to health.[1] There is an urgent need for new antimicrobial agents that allows us to tackle this problem in innovative ways.

Antimicrobial peptides (AMPs) have been identified as important leads for the next generation of antibiotics.[1b,2] The significant advantage of AMPs resides in the global mechanism of their action, which is significantly different from those of conventional antibiotics.[1d] AMPs display multifunctional properties, with implications for their application as potential therapeutic agents, because they represent an essential component of innate immunity.[3] They exhibit rapid killing, with a broad spectrum of activity against a large array of microorganisms including Gram-positive and Gram-negative bacteria, fungi and protozoan and metazoan parasites.[1b,4]

The unique and diverse group of AMPs is divided into several subgroups, on the basis of amino acid composition and structure.[1c,4c] Linear, cationic AMPs display a number of common characteristics including low molecular weight (10–50 amino acids) and amphiphilicity. The latter arises from the high content of positively charged amino acids (lysine, arginine, overall charge generally from +2 to +9) along with a substantial proportion of hydrophobic residues (≥30%).[2b,5] Both of these are key structural features that guide the antimicrobial effects of these peptides.

The electrostatic repulsion between the charged side chains renders the solution structures of the majority of cationic AMPs intrinsically disordered (ID) with no discernible secondary structure.[1c,5a,6] Upon membrane binding, an unstructured AMP undergoes a conformational change and folds into a well-or-

[a] M. Quemé-Peña, Dr. T. Juhász, Dr. J. Mihály, Dr. I. Cs. Szigyártó, C. Németh, Dr. Z. Varga, Dr. F. Zsila, Dr. T. Beke-Somfai
Institute of Materials and Environmental Chemistry
Research Centre for Natural Sciences, Hungarian Academy of Sciences
Magyar tudósok körútja 2, 1117 Budapest (Hungary)
E-mail: juhasz.tunde@ttk.mta.hu
beke-somfai.tamas@ttk.mta.hu

[b] Dr. K. Horváti, Dr. S. Bősze
MTA-ELTE Research Group of Peptide Chemistry
Hungarian Academy of Sciences, Eötvös Loránd University
Pázmány Péter sétány 1/A, 1117 Budapest (Hungary)

[c] J. Henczkó, B. Pályi
National Biosafety Laboratory, National Public Health Center
Albert Flórián út 2, 1097 Budapest (Hungary)

Supporting information and the ORCID identification numbers for the authors of this article can be found under https://doi.org/10.1002/cbic.201800801.

This article is part of the young researchers' issue ChemBioTalents. To view the complete issue, visit http://chembiochem.org/chembiotalents

dered—mostly α-helical—structure.[7] Because these peptides exert their action within the membrane environment, the membrane-associated conformational transition is believed to be a crucial step in mediating their biological activities. This structural transition could also be dependent on the lipid composition, leading to increased specificity towards membranes enriched in negatively charged species.[1d,8]

However, the in vivo action of these peptides is a complex issue, possibly including numerous types of interactions with small-molecule agents. Indeed, previous studies in our group have suggested that small molecules of both endogenous and synthetic origin can dramatically affect the structures of AMPs, potentially altering their mechanistic function, including their antimicrobial efficiency.[5a,9] Similarly, it has also been observed that several disordered AMP and protein sequences adopt ordered secondary structures induced by the lipid mediator lysophosphatidic acid;[10] this indicates that the presence and use of such interactions might be widespread in organisms, a phenomenon far from being understood.

To shed more light on this issue, this study has focused on CM15, a short, linear, natively unfolded, synthetic hybrid AMP combined from the silk moth cecropin A and the bee venom peptide melittin. CM15 displays a potent broad-spectrum antimicrobial activity, retaining the bactericidal effect of cecropins but lacking the strong haemolytic property of melittin.[3,5a,c,9] With a total charge of +6, it has a much higher average charge per residue than its congeners. The highly cationic N-terminal region and a mostly hydrophobic C-terminal region separate into a hydrophilic and a hydrophobic part upon helix formation (Scheme 1) coupled to membrane interaction. On the basis of the above factors, CM15 was used as a model peptide for preliminary screening of folding inducer effects of anionic drugs and biomolecules.[5a] Of the biomolecules and synthetic compounds tested on CM15, the therapeutic drug suramin was the most potent helix promoter,[5a] and so it was selected for this study as the most suitable candidate for addressing the more complex AMP–small molecule–lipid bilayer interactions. Suramin is a symmetrical, hexasulfonated naphthylurea used since 1920[11] as an anthelmintic, for treating onchocerciasis (African river blindness)[12] and sleeping sickness (African trypanosomiasis).[13] Suramin also shows anticancer and antiviral properties.[12a,14]

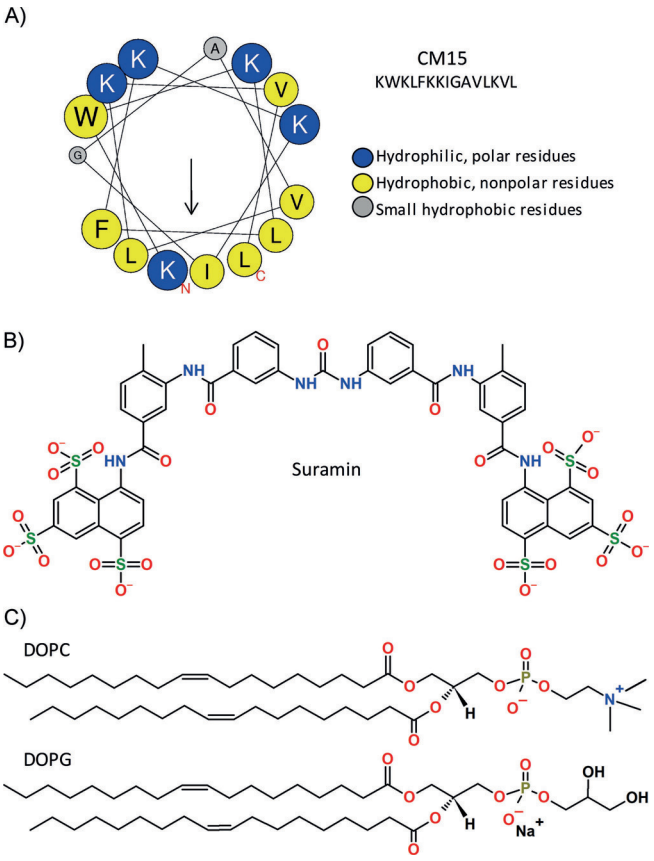

Scheme 1. Structures of the compounds used in the study. A) Helical wheel diagram of CM15 (KWKLFKKIGAVLKVL-amide), N and C stand for the N and C termini of the peptide. The helix plot was drawn with HELIQUEST.[15] B) Chemical structure of suramin. C) Chemical structures of the lipid components used in model membranes built up of DOPC (PC) and DOPG (PG). For mimicking mammalian and bacterial cell membranes, pure DOPC and DOPC/DOPG (80:20, *n*/*n*%) were used throughout the study. In the chemical structures, oxygen and nitrogen atoms are coloured red and blue, highlighting negatively and positively charged parts, respectively.

Using in vitro binding and functional assays, we characterised the interaction network of the CM15/suramin/membrane system. The results indicate that the drug affects not only the secondary structure of the AMP but also its membrane activity, and that this finally results in decreased antibacterial activity. This observation implies that as yet undetected side effects might be identified when drugs with similar characteristics are administered. Alternatively, it is also hoped that the insight gained might provide a potential aspect to exploit in the development of new strategies, in which AMP function might be altered or even increased in a controllable manner.

Tamás Beke-Somfai is a group leader in the Institute of Materials and Environmental Chemistry, Research Centre for Natural Sciences, Budapest. He obtained his M.Sc. (2001) in chemistry and Ph.D. in structural chemistry (2007) at Eötvös University, Budapest. He worked as a postdoc and guest researcher at Chalmers University of Technology, Gothenburg, Sweden (2008–2015). As a Marie-Skłodowska Curie fellow he returned to Budapest in 2015, leading the Biomolecular Self-Assembly group under the "Momentum" excellence programme of the Hungarian Academy of Sciences. His research involves investigation of natural and non-natural peptide assemblies, enzyme catalysis, polarised light spectroscopy and membrane–biomolecule interactions.

Results and Discussion

Circular dichroism study of structural changes in CM15 in the presence of suramin and liposomes

As previously reported,[5a] the drug suramin (Sur) has proved to be an effective folding inducer with the disordered membrane-active peptide CM15. To aid understanding of the structural effects of suramin on the interaction between CM15 and membranes, CD spectra in the presence of the interacting partners were collected.

The far-UV CD spectrum of free CM15 measured in buffer, with a single negative band at around 198–200 nm and no significant shoulder in the 210–230 nm region, indicates an intrinsically disordered state (Figure 1 A). This is in agreement with reported observations.[5a,16] On the basis of the results presented here and in previous studies,[5a] suramin triggers the disorder-to-order conformational transition of CM15. The characteristic positive/negative couplet corresponding to π–π^* transitions at 195 and 208 nm, as well as the negative band due to the n–π^* transition at 222 nm (Figure 1 A), suggest α-helical folding of CM15.[17] Secondary structure analysis also indicates increased helix content (Table S1 in the Supporting Information).[5a] These spectral transformations occurred promptly after addition of the drug and are related to rapid interaction.

Moreover, the relatively weak CD signals might be indicative of complex formation accompanied by aggregation; this has been verified by dynamic light scattering (DLS) measurements detecting particles on the micrometre scale.[5a] It is to be noted that the intensity ratio of the CD values at 222 and 208 nm is below $\approx$0.9 for non-interacting α-helices. In line with CD data, this value is >1 for the CM15/suramin mixture (Figure 1 A), thus suggesting oligomerisation of the peptide chains. In view of the net charges of $+6$ and -6 of CM15 and suramin, respectively, neutral 1:1 complexes could easily assemble into higher oligomers or aggregates as suggested previously.[5a]

Structural order gained upon interaction with membranes was probed with dioleoyl–phosphatidylcholine (DOPC, or PC) and dioleoyl-phosphatidylglycerol (DOPG, or PG) liposomes, mimicking electrostatic features of mammalian and bacterial biomembranes, respectively. Addition of neutral PC liposomes to CM15 caused the main negative band of the peptide to be red-shifted (from 198 to 203 nm), together with an intensity decrease, and the unresolved negative shoulder at 222 nm to become more pronounced (Figure 1 A). This partial helical folding could be the result of a weak, rather hydrophobic interaction lacking electrostatic attraction between the zwitterionic lipids and the peptide.[5b] The outer leaflet of the mammalian cell membrane is exclusively composed of neutral, zwitterionic phospholipids, towards which charged peptides such as CM15 show lower affinity;[18] that is also why ionic AMPs are less toxic towards mammalian cells.[4c,8b,c] In contrast, upon addition of negatively charged PC/PG liposomes, the ID peptide folds into a definite helical conformation (Figure 1 A). Helix formation is also supported by the estimated $\approx$40% helix content for the lipid-loaded CM15 (Figure 1 B and Table S1). In this case, the driving force behind the folding could be the combination of electrostatic interactions between the positively charged residues of the peptide and the negatively charged PG head groups, as well as hydrophobic interactions between the nonpolar side chains and the hydrophobic core of the lipid bilayer.[5b,18]

To test the effect of suramin on lipid-bound peptide, titration with the drug was carried out in the presence of model membranes. In sharp contrast to the case of the free peptide, where addition of the drug resulted in elevated helix content, which saturated at 1:1 molar ratio, for the lipid-bound CM15, the suramin dependence was remarkably different (Figure 1 B). With increasing suramin concentration, the helix content first reduced below the value of the lipid-free state in both types of vesicles, and this was then followed by a signal increase resulting in an approximately doubled helix fraction at 1:2 molar ratio, relative to the suramin-free state (Figure 1 B). However,

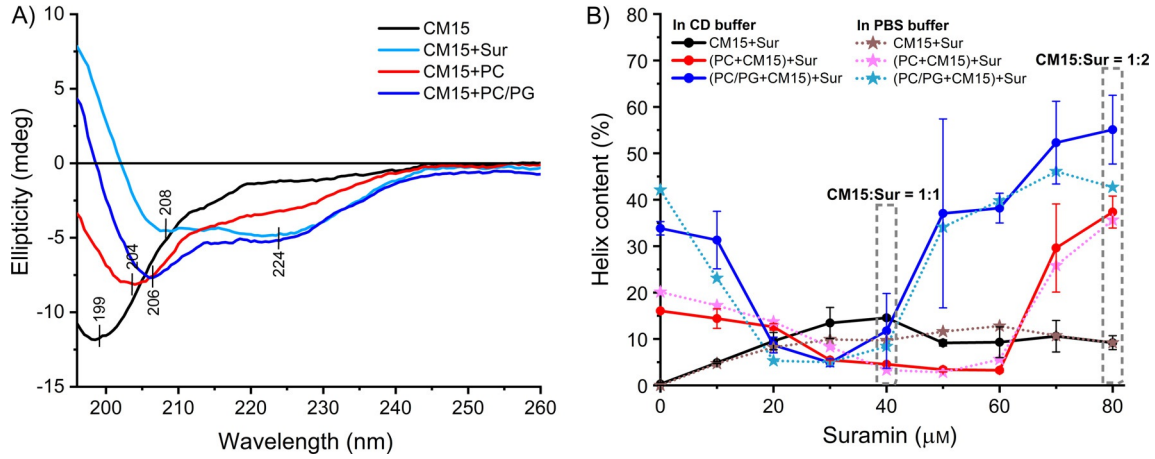

Figure 1. Structural changes of CM15 in the presence and in the absence of model membranes and suramin, studied by CD spectroscopy. A) Far-UV CD spectra were taken at peptide, suramin and lipid concentrations of 40, 40, and 635 μM, respectively. B) Effect of suramin on the helix content of free and membrane-bound CM15. The peptide (40 μM) was titrated with suramin in the absence and in the presence of liposomes (635 μM total lipid) with use of CD buffer or PBS (for the compositions see the Experimental Section). Helix content was estimated with the aid of the BestSel online tool.[30] Data are means ± SEMs, two series of titrations were carried out with CD buffer, and a single titration in PBS was performed as a control.

differences between the two liposome types were also revealed. For the neutral PC system, the helical content rose at high suramin ratios (>60 μM, Figure 1B). The phenomenon could be explained in terms of nonspecific association of suramin above a threshold concentration on the lipid bilayer rendering the neutral surface negatively charged, and this might facilitate peptide binding and induce helical folding.

It should also be noted that titration curves following the same trend were obtained both in the presence and in the absence of sulfate ions, resembling drug sulfonate groups (Figure 1B). Thus, it is evident that the sulfate moiety alone is not enough to trigger the peptide conformational changes induced by suramin, in which relative spatial arrangement of the negatively charged groups as well as the separating rings act in concert.

Altogether, these findings suggest that suramin interacts with CM15 even in the presence of lipid bilayers and governs peptide conformation in a concentration-dependent manner. For examination both of peptide structural changes and of charge neutralisation effects, mixtures with peptide/suramin ratios of 1:1 and 1:2 were investigated throughout this study.

To determine the relative affinities of the peptide towards lipid and small-molecule binding partners, three-component mixtures differing only in the order of mixing of the components were tested. In general, spectral features of the liposome-containing samples more closely resemble those of the suramin-loaded peptide than those of the lipid-bound state, and indicate random coil-to-helix transition (Figure 2 and Table S1). However, clear differences potentially attributable to the binding preference of the peptide could be observed. For systems with a CM15/suramin ratio of 1:2 (Figure 2B and D), comparable spectra were obtained for the two-component CM15·suramin complexes and the three-component mixtures in which the peptide competes for the partners, (Sur + lipid) + CM15, thus suggesting the prevalence of peptide–drug binding over the lipid interaction. However, the strongest signal, exceeding intensities for the pure CM15·suramin complex, was detected with PC/PG liposomes when suramin was added to the lipid-bound peptide (Figure 2D); this argues for the highest apparent ordered peptide fraction with possibly the lowest level of aggregation for the (CM15 + PC/PG) + Sur mixture. This also points to the ability of suramin to enhance helical conformation even when the peptide is already attached to the lipid bilayer. Alternatively, variations in the spectral intensity might be coupled to aggregation induced by the small-molecule compound. Consistent with these observations, although the helical character of the peptide is clear, the intensity of the CD signal is rather low for most of the three-component mixtures but especially with the 1:1 CM15/suramin ratio (Figure 2A and C); this could be indicative of higher levels of aggregation.

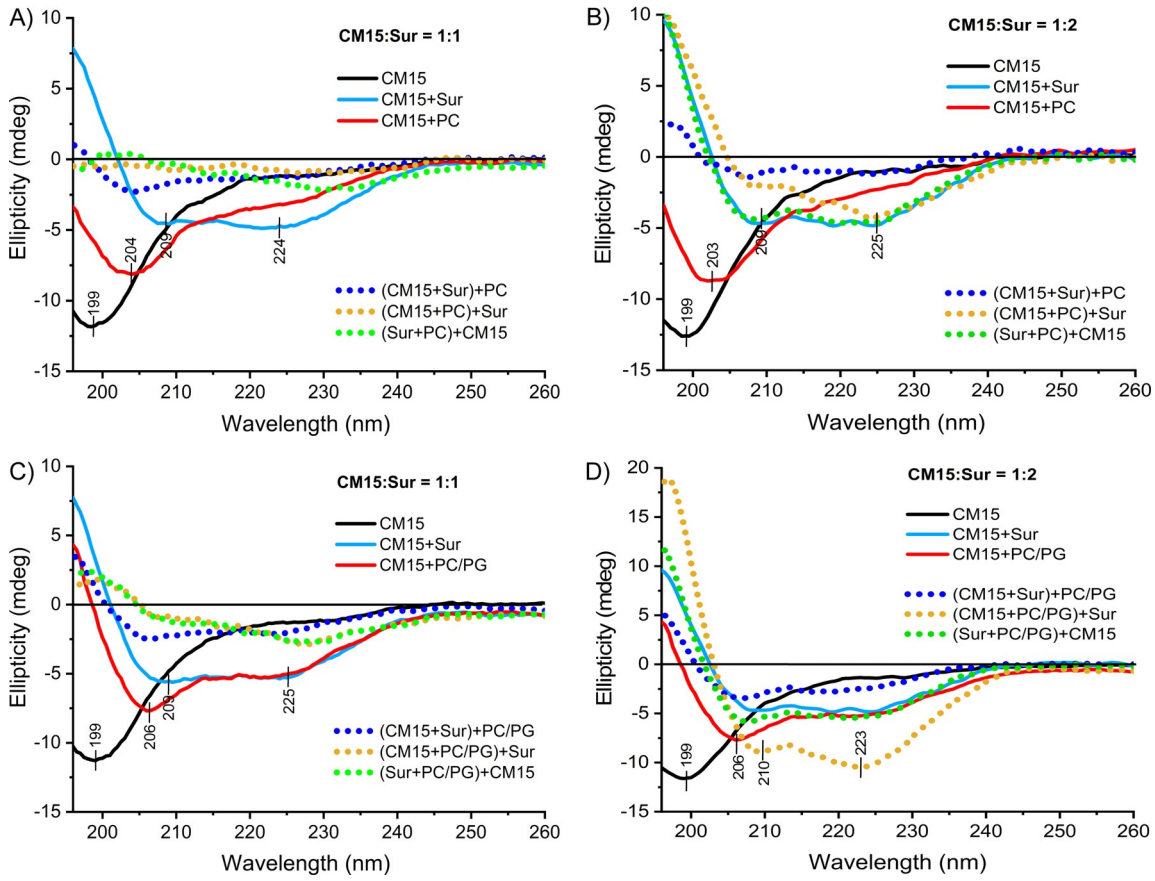

Figure 2. Far-UV CD spectra of CM15 in the presence and in the absence of model membranes and suramin. Spectra were collected at 40 μM peptide A), B) with PC, and C), D) with PC/PG liposomes (635 μM total lipid) at CM15/suramin ratios of A), C) 1:1, or B), D) 1:2. The order of addition in the three-component system was varied so that the preincubation of the two compounds in parentheses was initially performed, with the third compound then being added.

From the CD spectral features observed for the two- and three-component systems, additional information about peptide binding characteristics could be derived. The π–π^* band minimum of the PC/PG-bound CM15 is below 210 nm, whereas for the suramin-associated peptide it is at around 210 nm (Figure 2C and D). This wavelength shift could reflect polarity changes in peptide backbone surroundings. Specifically, the hydrophobic environment provided by PC/PG liposomes could increase the excitation energy of the π–π^* transitions, resulting in a blue shift. Conversely, the more polar aqueous phase around the CM15·suramin complexes could cause a red shift of the π–π^* peak. In light of this consideration, spectral features witnessed for three-component mixtures showing non-reduced signals—Figure 2B and D, (Sur + lipid) + CM15 and (CM15 + PC/PG) + Sur—are consistent with a binding scenario in which peptide chains are not inserted into the nonpolar interior of the lipid bilayer but rather are exposed to the bulk aqueous phase. Furthermore, in view of suramin association to the vesicles as suggested above, peptide–suramin interaction might occur at the liposome surface.

CM15·suramin complex aggregation revealed by DLS and electron microscopy

To monitor formation of molecular aggregates, DLS measurements were conducted. As previously indicated,[5a] large associates appeared in the case of the two-component CM15/suramin system. They showed hydrodynamic diameters in the low-micrometre range, also confirmed here for both 1:1 and 1:2 peptide/suramin ratios (Figure 3, Tables S2 and S3). The phenomenon was explained in terms of mutual charge neutralisation in complexes made up of the cationic CM15 and its anionic partner, resulting in less hydrophilic adducts that were prone to aggregation in the aqueous environment.[5a]

Peptide binding to the lipids induced no detectable changes in the correlation function, so a liposome size of 100 nm was determined for the vesicle/peptide mixtures. Similarly, addition of suramin to the model membranes caused no perturbation of the curves. However, for the three-component systems, a shift of the correlation function to higher decay times is consistent with formation of aggregates with diameters greater than 100 nm. The estimated aggregate size, in the high-nanometre to low-micrometre range, is similar to that measured for CM15·suramin complexes. Large-sized associates were clearly detected in the presence of PC liposomes, but this was not so pronounced with PC/PG liposomes. In general, mixtures of preincubated peptide and drug with subsequent addition of lipid vesicles showed the greatest propensity to form large aggregates. As an exception to this, all three-component systems displayed large-sized particles in the presence of neutral PC liposomes, thus highlighting the importance of peptide–drug charge neutralisation in effective assembly. The association process is also regulated by the CM15/suramin ratio, with the size distributions of the aggregates being found to be narrow-

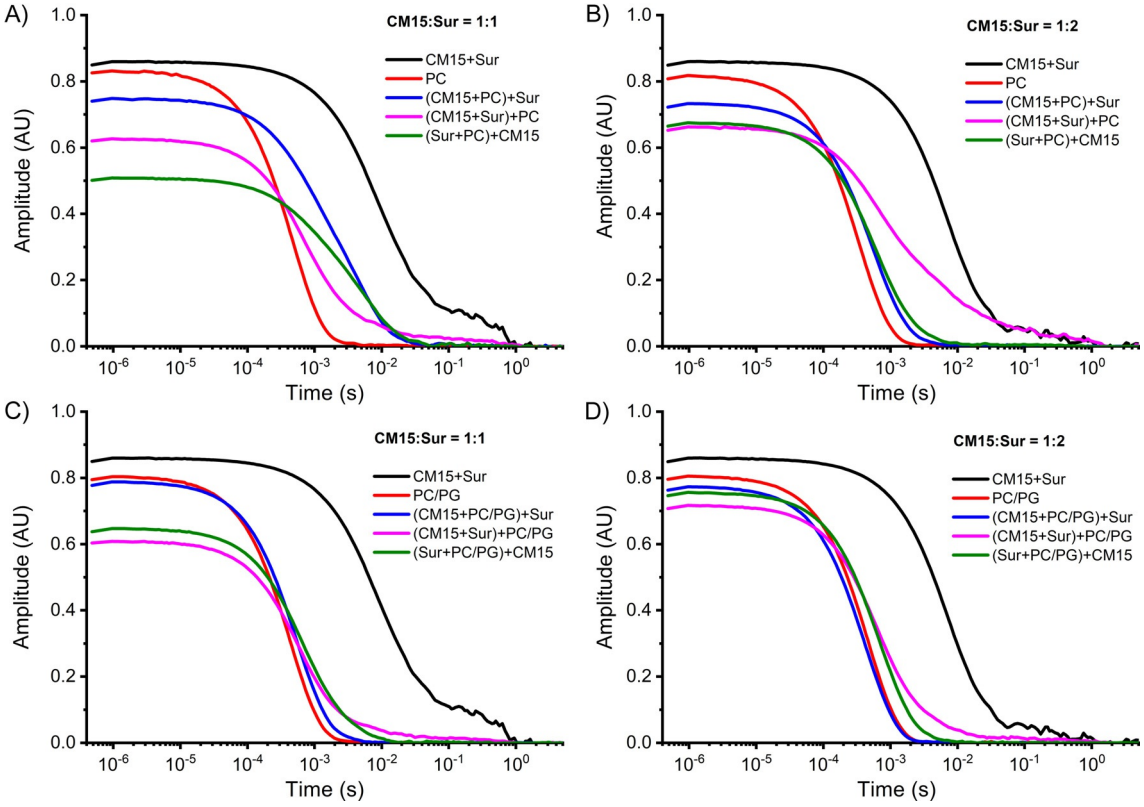

Figure 3. Peptide–drug assembly in the two- and three-component systems monitored by DLS. Correlation functions are shown for mixtures with CM15/suramin ratios of A), C) 1:1, and B), D) 1:2, in the absence and in the presence of A), B) PC, and C), D) PC/PG liposomes. Peptide, suramin and lipid concentrations are 20, 20 or 40, and 635 μM, respectively. For more details see Tables S2 and S3.

er in the case of the 1:2 ratio than in that of the 1:1 ratio (Tables S2 and S3). In line with this, no such dependence on the molar ratio was observed in the case of the anionic PC/PG vesicles.

Aggregate formation was further investigated by transmission electron microscopy (TEM), providing additional information on the morphology of the CM15·suramin complex. Consistent with the DLS results, TEM images for both 1:1 and 1:2 peptide/drug ratios (Figure 4) showed formations of up to 1–2 μm in diameter with a characteristic morphology. These displayed networks of sphere-like building blocks of ≈50 nm interconnected by rather linear regions. A similar associated state, depicted as a beadlike branched morphology, was reported for the anticancer/antimicrobial peptide LL-37 in a complex with self-RNA as detected by phase-contrast-light, scanning-electron and confocal fluorescence microscopy.[19] These findings suggest that cationic amphiphilic peptides such as CM15 and LL-37 might easily form complex aggregates with anionic partners bearing aromatic rings with limited structural flexibility, such as drugs or nucleotides. It should be noted that particles with this morphology are typical for the CM15·suramin complex but were observed neither in peptide-only nor in drug-only solutions.

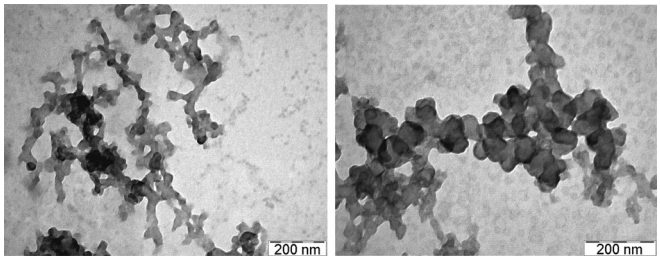

Figure 4. Morphology of the CM15·suramin complex imaged by TEM. Micrographs of the mixtures stained with phosphotungstic acid were taken at CM15/suramin ratios of 1:1 (left) and 1:2 (right). Peptide and suramin concentrations in the solutions prior to drying were 20 and 20 or 40 μM, respectively.

Tryptophan fluorescence indicates altered environments in different lipid complexes

To obtain additional information on the CM15–suramin interaction in the presence of various lipid bilayers, fluorescence spectroscopy measurements were performed. Here we exploited the intrinsic tryptophan fluorescence of the peptide, which sensitively reports binding events that lead to polarity changes in the local fluorophore environment.

The spectrum of the free peptide is characterised by an emission maximum at 357 nm (Figure 5), consistent with a water-accessible tryptophan of a disordered peptide. Upon addition of the liposomes, the membrane-bound state was easily detectable through the blue shift of the maximum. This phenomenon is typical for a tryptophan residue inserted in a more nonpolar environment shielded from the aqueous phase. The effect was more pronounced, accompanied by a significant intensity increase, in the case of the negatively charged PC/PG liposome. In contrast, the rather wide maximum in the case of the PC-bound peptide suggests the coexistence of two tryptophan populations with different environments. These results agree well with stronger peptide binding associated with more intimate interaction with PG-containing bilayers than in the case of the neutral PC liposome, and are also in line with the CD-based considerations above.

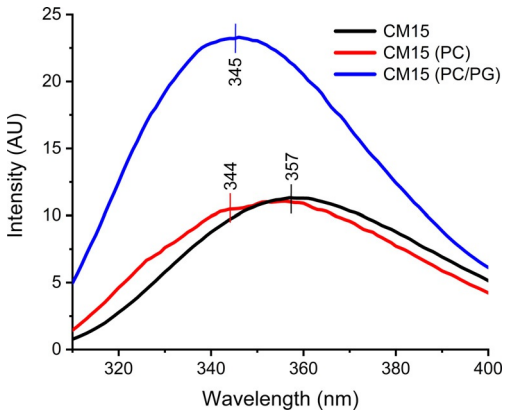

Figure 5. Fluorescence emission spectra of CM15 in the absence and in the presence of model membranes. Peptide and lipid concentrations were 1 and 100 μM, respectively.

Titration of CM15 with suramin resulted in a reduced emission intensity, indicating a nearby quencher group in the complex (Figure 6A). If the structure of suramin (Scheme 1) is considered, the aromatic naphthyl moieties could account for the effect, although ligand-binding-induced helical folding could also lead to tryptophan quenching due to enhanced rigidity and closer proximity of adjacent side chains.[20] Nevertheless, the moderate dose-dependent intensity decrease, leading to almost complete fluorescence loss at 50 μM drug concentration (Figure 6A), is characteristic for the CM15–suramin interaction. Similarly, nearly complete loss of fluorescence upon addition of suramin was reported for the recombinant prion PrP protein and attributed to suramin-induced aggregation,[21] a phenomenon also detected here for CM15, as discussed above.

For purposes of comparison, the same experiment was carried out with the non-binding tryptophan control *N*-acetyltryptophanamide (NATA), which does not form stable complexes with suramin and can consequently reflect dynamic quenching and/or inner filter effects. In this case (Figure 6B) intensity loss was much weaker, and the lack of static binding of NATA to liposomes or suramin is evident from the slight linear suramin-dependent intensity decrease, which occurred to the same extent both in the presence and in the absence of lipid vesicles. Thus, the difference in quenching efficiency observed on comparing the effects of suramin on NATA and CM15 could be accounted for by the peptide binding of the drug.

When suramin titration was performed on lipid-loaded peptide, more effective quenching was observed than in the case of the lipid-free state, thus suggesting a different peptide–drug binding mode (Figure 6B). For the PC system, the fluores-

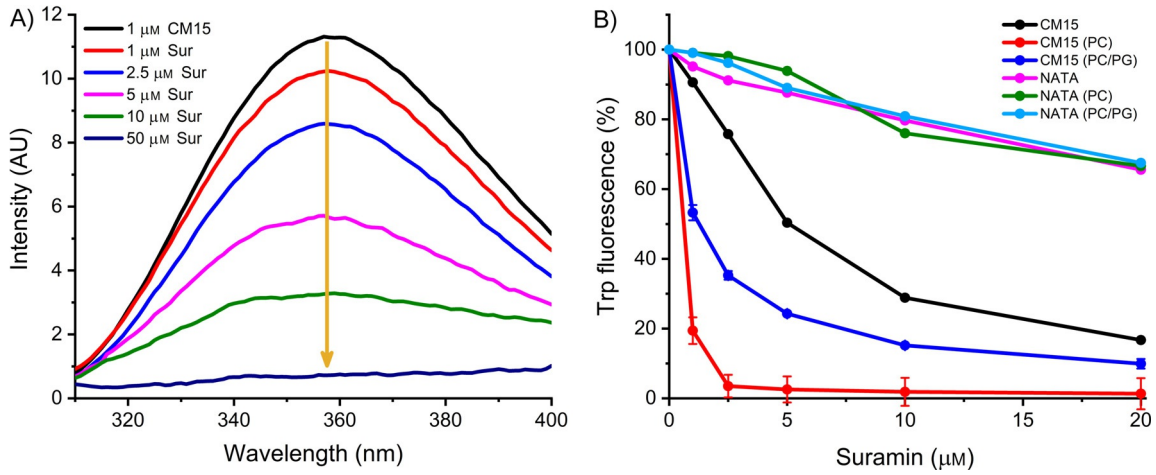

Figure 6. Peptide fluorescence study of suramin binding to CM15 in the absence and in the presence of liposomes. A) Fluorescence emission spectra of CM15 (1 μM) upon addition of suramin. Arrow indicates increasing drug concentrations. B) Normalised maximum emission intensities of CM15 (1 μM) and the control NATA (1 μM) as a function of suramin concentration. Note that error bars for the peptide titration points are mostly smaller than symbol size (data are means ± SEMs, $n = 2$).

cence loss was ≈85% at 1:1 and complete at a peptide/suramin ratio of 1:2.5. PC/PG liposomes showed intermediate behaviour closer to that of the free peptide than that of the PC-bound state. A possible explanation for the phenomenon could be binding of suramin to the lipid bilayer separately from the peptide and/or to the vesicle-bound peptide, resulting in a better relative positioning of the putative suramin quencher group for accessing the peptide fluorophore. If the suramin naphthyl groups were assumed as the quenchers, detection of more efficient quenching in the case of the PC-bound peptide would require tryptophan situated closer to suramin and/or in a more suitable relative orientation of the two rings on the two components enabling better contact than in the case of the pure peptide·drug complex. This could relieve some "lifting out" of the lipid-loaded peptide inserted to some depth into the bilayer, which could be easier in the case of the PC-bound peptide, with a looser contact to the vesicle. In contrast, the tryptophan in the peptide bound more tightly to the PC/PG liposome could remain more firmly incorporated, although still located closer to the suramin quencher part. In the latter case, drug binding would probably be less favoured because of electrostatic repulsion between the negatively charged suramin sulfonyl and PG head groups. Nevertheless, this binding mode assumes preferred interaction between the N-terminal part of CM15 and the middle part of suramin (Scheme 1) in the CM15·suramin complex, and this was indeed predicted by means of a computational approach in our group.[22] Moreover, similar binding characteristics involving the membrane-associated drug could be deduced from CD findings (see above) and from IR spectroscopy experiments (see below).

Although the ability of suramin to quench a fluorophore such as a tryptophan has been demonstrated here and is reported in ref. [21], suramin also has intrinsic fluorescence properties related to its naphthylamide moiety. When excited separately from tryptophan at 315 nm, suramin emission with a maximum near 400 nm showed remarkable enhancements of up to tenfold in the presence of protein binding partners.[23] However, when excited at 295 nm—the wavelength used here for exciting tryptophan—the weak emission peak developing at ≈400 nm showed no sensitivity to drug interactions with CM15 or vesicles (data not shown).

In summary, fluorescence data suggest perturbed CM15–suramin interaction with different relative conformations of the peptide towards the binding partners in the presence of lipid bilayers. Titration results obtained for lipid-bound CM15 are not compatible with simple peptide displacement from the vesicles by suramin.

Peptide partition between liposome-bound and suramin-complexed states suggested by IR spectroscopy

The interaction between CM15 and lipid assemblies such as vesicles has been studied by means of IR spectroscopy by several groups.[2d,24] Bastos et al.[24d] investigated the interaction between CM15 and liposomes formed from saturated lipids that were also shorter than those (PC/PG) used here. By monitoring lipid carbonyl stretch as a function of increasing peptide concentration, it was reported that the bilayer retained significant order in the presence of the peptide.

Parts of IR spectra involving lipid carbonyl (ca. 1735 cm^{-1}) bands, as well as peptide amide I (ca. 1660 cm^{-1}) and amide II (ca. 1545 cm^{-1}) bands of CM15–liposome associates (Figure 7 A) were analysed. No drastic changes relating to the lipid order in the bilayer were observed. The small shift of lipid carbonyl bands (from 1736 to 1735 cm^{-1}) in the presence of the peptide suggests that the polar/nonpolar interface in the lipid bilayer could be involved in the interaction in the cases both of PC and of PC/PG vesicles.

More pronounced changes were witnessed in the amide I band of the peptide upon lipid binding. Beside the main band at 1660 cm^{-1} assigned to the disordered/helical fraction, a new

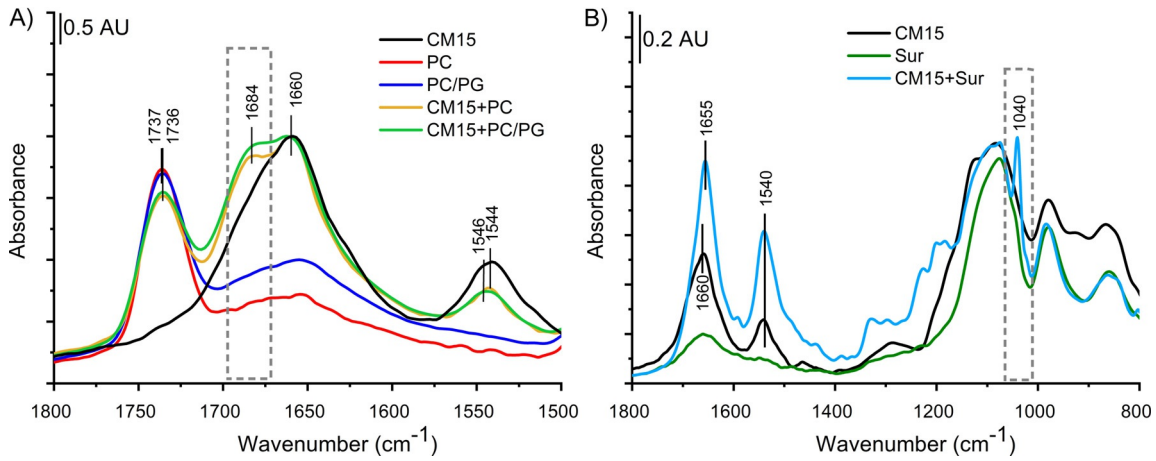

Figure 7. IR study of CM15 binding to model membranes and suramin. A) Amide I and II regions, as well as lipid carbonyl bands, recorded for CM15/liposome systems. B) Formation of CM15·suramin complex indicated by the appearance of an extra band at 1040 cm^{-1}.

band component appeared at around 1684 cm^{-1} in the presence of liposomes. In an early study on interactions between melittin or melittin fragments and PC vesicles, Brauner et al.[25] observed very similar spectral features. They speculated that the band at 1685 cm^{-1} arose from peptides assembled at the lipid surface in an extended conformation.[25]

In general, there is some controversy relating to results available for CM15 and other membrane-active peptides when peptide orientation relative to the bilayer is considered. It has been argued that perpendicular insertion connected mainly to pore formation by the surface-associated peptide might occur above a threshold peptide concentration and peptide/lipid ratio.[3,5c,24d]

The structural changes associated with CM15–suramin interaction can also be monitored by IR spectroscopy (Figures 7 and 8). An important advantage of the method is that the signal is not complicated by spectral perturbations due to the presence of aggregates. Changes in the amide I and amide II bands (Figure 7A) suggest a protein-like complex structure with predominant helical conformation (corroborated by the amide I peak centred at 1655 cm^{-1}) connected to suramin-induced oligomerisation/aggregation. Similar observations have also been made by other methods.[5a] In addition, a remarkable feature of the CM15·suramin complex is a sharp peak at 1040 cm^{-1} that is markedly separated from the buffer phosphate vibrations (Figure 7B). This band can be assigned to the in-phase S–O stretching of the sulfonyl groups in the complexed suramin, as also observed for suramin oligomers.[26] Thus, the extra band at 1040 cm^{-1} could be used as an IR marker for identification and approximate quantification of CM15·suramin complex formation. We have to point out that at the suramin concentrations used—80 and 160 μM—no such local crowding was detected in the absence of CM15. This is in agreement with NMR data that support the prevalence of monomers at 0.5 mM concentration but oligomerisation at 5 mM.[27]

On the basis of the spectral changes experienced for the two-component systems, in the three-component mixtures we focused on the evolution of the amide I band component at 1684 cm^{-1}, as well as on the band at 1040 cm^{-1}, as measures of the peptide–lipid and peptide–drug interactions, respectively.

Firstly, liposome systems with 1:2 peptide/suramin ratios were analysed (Figure 8). These revealed substantial differences when the mixing order of the components was varied. Upon addition of suramin to PC-bound CM15, the intensity of the shoulder amide I band at 1684 cm^{-1} decreases (Figure 8A), indicating competition of lipid and drug for the peptide. However, when suramin is added first to CM15 or PC, suppression of the amide I band component is nearly complete (Figure 8A), thus suggesting higher affinity of CM15 towards the drug. A similar trend was observed for the extra band at 1040 cm^{-1} (Figure 8B and Table S4).

From the band intensities, the largest amount of CM15·suramin complex was formed when the peptide and the small-molecule compound were mixed first. In the case of administration of suramin to the PC-bound peptide, the affinity of CM15 towards the liposomes is, however, only partially abolished, in parallel with reduced CM15·suramin complex formation.

When addition of suramin to liposomes was followed by incorporation of the peptide, CM15·suramin complex formation was still remarkable and no redistribution towards liposomes was witnessed. A possible explanation for this could be lipid binding of CM15 being strong enough to interfere with suramin interaction, so the liposome-loaded peptide cannot participate in complex formation with the drug. However, this binding scenario is not in full agreement with CD and DLS results indicating a significant fraction of CM15/suramin associates in the presence of neutral vesicles, which points to a binding event in which suramin can interact with liposomes and/or lipid-bound peptide as suggested by the CD and fluorescence results. Indeed, liposome-associated suramin causes perturbation of the lipid head group region, as indicated by a shift of the lipid asymmetric phosphate vibration (νPO_{as}) at 1240–1250 cm^{-1}.

With reduced suramin concentrations at the CM15/suramin ratio of 1:1 in the PC system (Figure S2), weaker peptide–liposome interaction was observed in all of the three-component

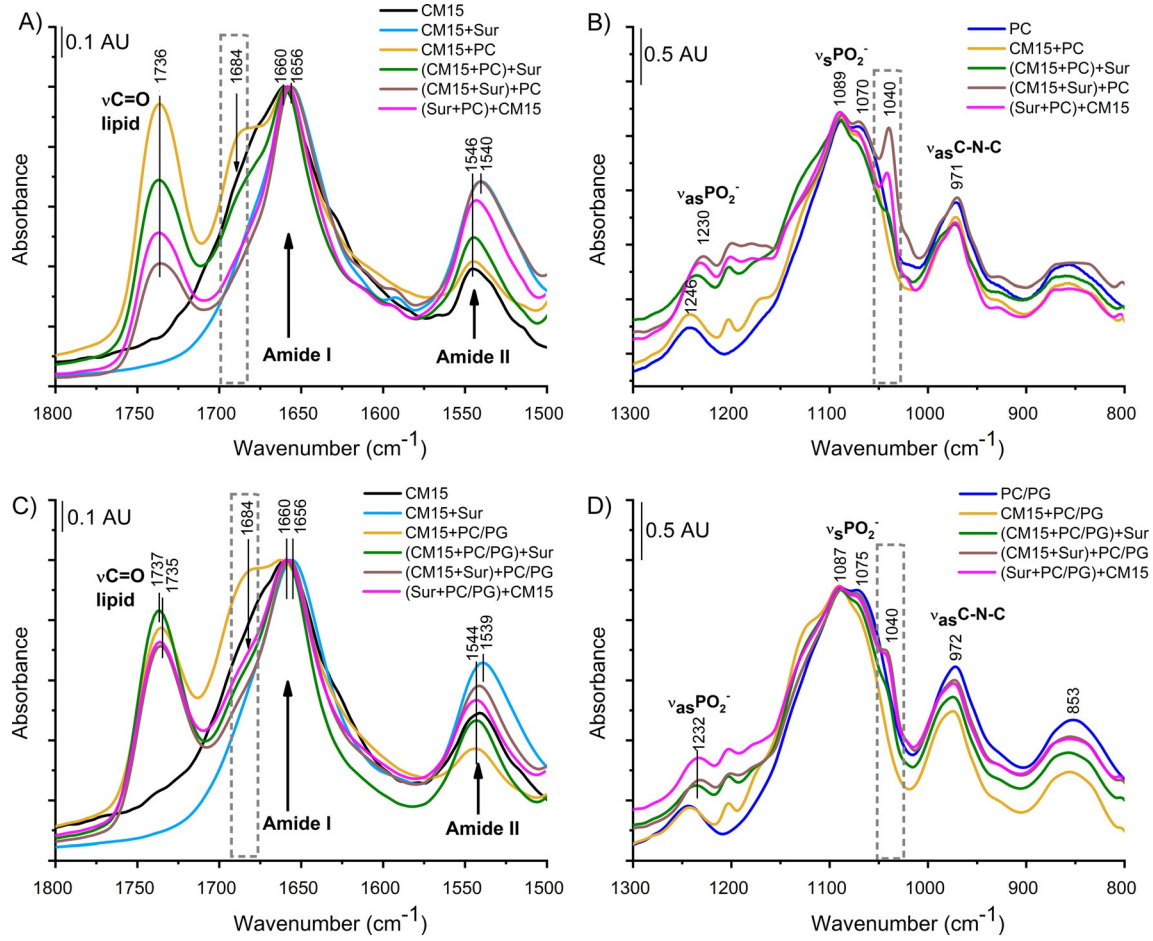

Figure 8. IR study of CM15 interactions in the presence of model membranes and suramin. A), C) Amide I and II regions and lipid carbonyl band. B), D) Formation of CM15·suramin complex indicated by the appearance of an extra band at 1040 cm^{-1}. ATR FTIR spectra were collected for dry films produced from solutions containing CM15 (80 μM), suramin (160 μM) and PC or PC/PG liposome (1.3 mM lipid).

mixtures, as indicated by a decline in intensity of the marker band at 1684 cm^{-1} and the shift of the lipid ester carbonyl band from 1736 to 1737 cm^{-1} (Figure S2 A). The latter suggests a slight lifting of CM15 from the polar/nonpolar boundary of the bilayer upon suramin addition. On the other hand, the formation of the CM15·suramin complex is less significant (Figure S2 B) than in the 1:2 CM15/suramin case (Figure 8 B). Nevertheless, the largest amount of peptide·drug complex was indicated when vesicles were added to the CM15/suramin mixture (Table S4).

With use of the PC/PG liposome system to mimic the negative charge of a bacterial membrane, both similarities to and differences from the neutral PC system were found. At a 1:2 peptide/suramin ratio (Figure 8), addition of suramin diminishes the amide I band shoulder at 1684 cm^{-1} significantly but not completely (Figure 8 C). Furthermore, the marker band of CM15–suramin association at 1040 cm^{-1} (Figure 8 D) is less pronounced (Figure 8 B). This is in line with the considerations above: namely the binding of CM15 to negatively charged liposomes being stronger than that to neutral lipids, so peptide·drug complex formation is more hindered in the former case (see also Table S4). From these results, it can be concluded that in the three-component systems there is competition for CM15 between binding to the liposome surface or complex formation with suramin. However, the (CM15 + PC/PG) + Sur mixture behaves exceptionally. For this system, both peptide interactions seem to be diminished, according to reduced band intensities at 1685 and 1040 cm^{-1}. Moreover, a slight shift of the lipid carbonyl band from 1735 to 1737 cm^{-1} is observed; this occurs only for this mixture combination.

In contrast to PC/PG liposome systems with a 1:2 peptide/suramin ratio, no shift of the lipid carbonyl group was observed for any mixture with a 1:1 ratio (Figure S2 C). Alterations in the 1684 cm^{-1} marker band suggest that in cases in which suramin is added to the PC-bound peptide, binding of CM15 to the liposome is still strong (Figure S2 C). Simultaneously, formation of CM15·suramin complex is also hindered, as confirmed by the significant intensity loss of the "complex marker" band at 1040 cm^{-1} (Figure S2 D and Table S4).

To summarise the findings obtained from IR measurements, our results point to dominant peptide–drug interaction when the lipid is added to the preformed CM15·suramin complexes. This preference is stronger at a CM15/suramin ratio of 1:2 and more relevant for the neutral PC system than for the charged PC/PG system. Vesicle attachment of CM15 could be strong enough to inhibit CM15·suramin complex formation; however,

interaction with suramin could result in peptide being lifted from the bilayer interior.

Binding determinants in the three-component systems

By combining the results obtained from the biophysical measurements, we can conclude a general binding scenario in three-component CM15/suramin/lipid systems in which CM15 forms a complex with suramin at the expense of binding to liposomes. However, not all spectral changes observed could be explained simply in terms of peptide displacement. Perturbations in the lipid head group region detected by IR spectroscopy and suggested by fluorescence quenching point to possible binding of suramin to the vesicles or even to lipid-bound peptide, allowing the formation of dynamic complex associates. In these assemblies, the peptide could be extruded from the polar/nonpolar boundary of the lipid bilayer but might preserve looser contact with the less buried regime of the lipid head group region facing the aqueous phase.

Moreover, our findings point to the importance of mixing order in peptide binding preference: that is, the binding partner that comes into contact with CM15 first. Peptide interaction with the small-molecule compound could dominate over liposome binding when the lipid is added to preformed CM15·suramin complexes. However, the binding preference is also controlled by peptide/suramin ratio as well as by vesicle composition, mainly driven by electrostatics. CM15 and suramin bear +6 and −6 net charges, respectively, so complex formation could be initiated by electrostatic attraction between peptide and drug. Consistently with charge neutralisation at an equimolar ratio and the negative overall charge of the complex at higher suramin concentrations, higher degrees of peptide partition towards complex formation with suramin leading to more significant aggregation were detected at 1:1 CM15/suramin ratio and in the case of the neutral liposome system. In contrast, vesicle attachment of CM15 could inhibit interaction with the drug when suramin meets the peptide associated tightly to the negatively charged membrane.

Our results suggested that electrostatic forces play a pivotal role in the initiation of peptide binding and assembly. This is consistent with previous studies in which it was assumed that electrostatics are a key factor in AMP–membrane interactions.[24d] However, in view of the amphiphilic nature of all partners (CM15, suramin, lipids), hydrophobic interactions could also contribute to the binding energetics. Indeed, CD spectra, tryptophan fluorescence and lipid carbonyl vibration indicated peptide regions residing close to the nonpolar interior of the lipid bilayer. In contrast, CD and IR spectroscopic results suggested a more polar environment for suramin-bound CM15 even in the presence of vesicles.

Variations in peptide structure monitored by CD and IR spectroscopy are compatible with a reduced content of the membrane-active peptide conformation in the presence of suramin, with this appearing to be valid even when the ability of suramin to interact with biomembranes is taken into account. To test the biological relevance of the above interactions and their potential in altering bioactivity, in vitro antibacterial and cytotoxicity assays were performed.

Altered antibacterial activity and cytotoxicity of CM15 in the presence of suramin

To understand the biological relevance of the AMP·drug complex formation, antibacterial effects and cytotoxicity on human cells were probed with CM15 premixed with suramin.

On the tested *Escherichia coli* strain, CM15 showed a remarkable antibacterial effect, as indicated by the fact that no bacterial growth was detected at peptide concentrations as low as 5 μM. In the presence of suramin, however, the peptide's efficiency was significantly decreased, with bacterial growth being observed even at higher CM15 concentrations of 10–40 μM (Figure 9A). To provide a more detailed picture on the effects of suramin, bacteria were treated with 5 μM peptide preincubated with excess suramin. A strong impact of the drug on the antibacterial efficacy of CM15 is evident, with significantly greater amounts of the bacterial cells surviving when CM15 was added with suramin (Figure 9B). Furthermore, increasing suramin concentrations resulted in higher relative bacterial growth. Specifically, this value at a peptide/suramin ratio of 1:2 was approximately half that at 1:8 (Figure 9B).

The membrane-disrupting activity of CM15 was also tested with human cells, specifically with MonoMac6 monocytes and red blood cells (RBCs). Cells were treated with CM15 in the absence or in the presence of suramin at 1:1 and 1:2 peptide/suramin ratios. With the monocyte cell line, CM15 alone was found to be cytotoxic at a relatively low concentration (IC_{50} = 7.6 μM, Figure 10A), whereas when it was administered together with suramin the effect was substantially decreased. Peptide

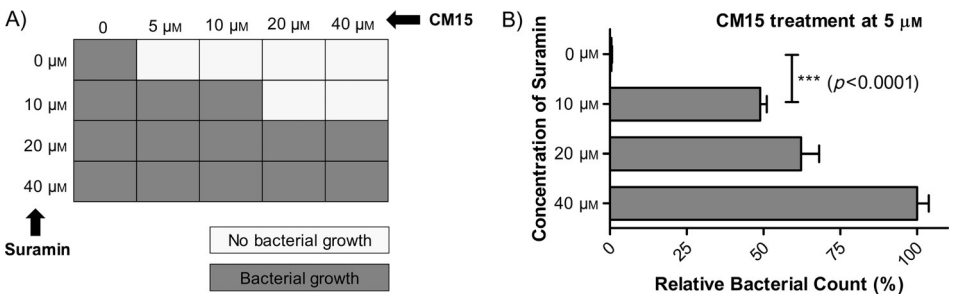

Figure 9. Antibacterial effect of CM15 in the presence and in the absence of suramin. A) *E. coli* treated with peptide/drug mixtures at various ratios. After 24 h incubation, no bacterial growth was detected in the CM15-treated wells. In contrast, when CM15 was added with suramin, visible bacterial growth was observed. B) Relative bacterial counts after treatment with 5 μM CM15 and various concentrations of suramin. Values are means ± SEMs (n = 4).

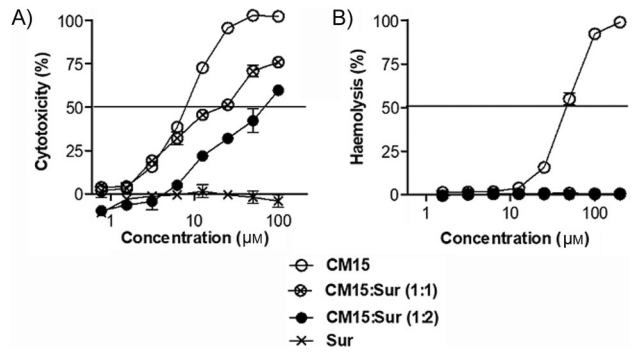

Figure 10. Cytotoxic and haemolytic effects of CM15 in the presence and in the absence of suramin. Cytotoxicity was measured with MonoMac6 human monocytes, and haemolysis was assayed with a suspension of human RBCs (4%, *v/v*). Data are means ± SEMs ($n = 3$). Note that error bars are often smaller than the symbol size, as well as the use of a logarithmic scale for the concentration. A) Significantly lower cytotoxicity was measured for CM15 administered together with suramin: IC_{50} values for CM15 alone and for CM15/suramin at 1:1 and 1:2 ratio are (7.6 ± 0.2), (19.6 ± 4.3), and (66.9 ± 4.5) μM, respectively, with $p = 0.0011$ for CM15 versus CM15/Sur (1:1) and $p < 0.0001$ for CM15 versus CM15/Sur (1:2). The effect was stronger when CM15 was mixed with suramin at higher (1:2) molar ratio. Suramin alone showed no cytotoxic effect ($IC_{50} > 100$ μM). B) Haemolytic activity of CM15 [$HC_{50} =$ (45.9 ± 1.6) μM] was abolished in the presence of suramin at both ratios applied ($HC_{50} > 200$ μM). Suramin alone showed no haemolytic effect ($HC_{50} >$ 200 μM). Note that data points overlap for Sur, CM15/Sur (1:1) and CM15/Sur (1:2).

cytotoxicity was impaired to a greater extent in the presence of an excess of suramin (IC_{50} values of 19.8 and 66.9 μM for 1:1 and 1:2 ratios, respectively, Figure 10A). On treatment of red blood cells, CM15 alone showed moderate cytotoxicity, with a HC_{50} value (peptide concentration at which 50% haemolysis occurred) of ≈45 μM (Figure 10B); this is consistent with the reduced haemolytic activity of the hybrid peptide relative to its parent melittin.[28] In the presence of suramin, no haemolysis was observed ($HC_{50} > 200$ μM, Figure 10B). It is to be noted that suramin alone at concentrations up to 100–200 μM showed no effect on these cells (Figure 10A and B), which indicates that reduced peptide cytotoxicity is directly connected to CM15·suramin complex formation.

In an early work, an effective concentration of 10 μM and typical drug dosage of 0.3 mM were reported for suramin.[11] In a recent study, patients were treated with suramin at plasma concentrations in the 140–190 μM range and the drug was cleared with a 40 d period half time.[29] Because suramin can reach high levels in vivo, the interactions investigated here are likely to occur in the human body.

Conclusion

We have investigated the structural and functional effects of the therapeutic drug suramin on the membrane-active antimicrobial peptide CM15 by a combination of several biophysical methods. On the basis of the structural data supported by in vitro binding assays, our findings are compatible with a model delineating formation of dynamic complex associates of the peptide populated in lipid-bound and/or drug-loaded forms. CM15 partition is governed mainly by charge neutralisation effects controlled by suramin-to-peptide ratio and lipid bilayer composition. We have also demonstrated that interaction with suramin changed peptide function appreciably, as illustrated by significantly reduced antimicrobial activity on Gram-negative bacteria and diminished cytotoxicity towards mammalian cells. In view of the low effective concentrations for both CM15 and suramin, high drug plasma levels during medical treatments and locally accumulated AMPs, suramin and AMP levels can fall in the range used in this study. On the bases of these findings and of several other small-molecule–AMP interactions demonstrated recently in our group, it is proposed that natural AMPs and host defence peptides will regularly experience alteration of their structures and functions in the complex in vivo environment—an aspect to be considered and potentially exploited during future treatments and drug design.

Experimental Section

Peptide solution: CM15 was synthesised in the solid phase by using an automated peptide synthesiser and a standard Fmoc/*t*Bu strategy. Peptide product was characterised by analytical RP-HPLC, mass spectrometry and amino acid analysis (see the Supporting Information for more details). Lyophilised CM15 powder (trifluoroacetate salt) was dissolved in high-purity water at the indicated concentration (not higher than 1 mM), aliquoted and stored frozen at −18 °C until use (no longer than a few weeks).

Suramin solution: Suramin powder (sodium salt, Calbiochem) was dissolved in high-purity water at the indicated concentration (not higher than 1 mM), aliquoted and stored frozen at −18 °C until use.

Lipid solutions: High-purity synthetic 1,2-dioleoyl-*sn*-glycero-3-phosphocholine (DOPC) and 1,2-dioleoyl-*sn*-glycero-3-[phospho-*rac*-(1-glycerol)] (DOPG) were purchased from Avanti Polar Lipids, Inc. Liposomes were prepared by the lipid thin-film hydration technique. Lipids were dissolved in chloroform (LabScan, Hungary) containing methanol (Reanal, Hungary, 50 vol%) and then evaporated with the aid of a rotary evaporator. The resulting lipid film was kept under vacuum for at least 8 h to remove residual traces of solvent. The dried lipid film was hydrated with the assay buffer. After repeated heating (37 °C) and cooling (−196 °C) steps (at least 10 times), the solutions were extruded through polycarbonate filters of 100 nm pore size (at least 11 times) with use of a LIPEX extruder (Northem Lipids, Inc., Canada). Final lipid concentration was 13 mM. For mimicking mammalian and bacterial cell membranes, pure DOPC and DOPC/DOPG (80:20, *n/n*%) were used throughout the study.

Assay conditions: To mimic physiological conditions, the assay buffer used throughout the study was isotonic phosphate-buffered saline [PBS, phosphate (10 mM), NaCl (137 mM), KCl (3 mM), pH 7.4], purchased from Sigma–Aldrich. For measuring CD spectra, a buffer free of chloride ions [CD buffer, Na phosphate (10 mM), Na_2SO_4 (100 mM), pH 7.0] was frequently used, allowing collection of spectra down to 190 nm.

In investigation of three-component systems, the order of addition of the components was varied. This involved preincubation of two compounds (Comp1 and 2) for 3–4 min, followed by the incorporation of the third one (Comp3). The corresponding labelling used throughout the text is (Comp1 + Comp2) + Comp3.

Circular dichroism (CD) spectroscopy: CD spectra were collected with a JASCO J-1500 spectropolarimeter at room temperature in 0.1 cm path-length cylindrical quartz cuvettes (Hellma, USA). Peptide CD data were collected in continuous scanning mode between 190 and 260 nm at a rate of 50 nm min^{-1}, with a data pitch of 0.5 nm, response time of 4 s, 1 nm bandwidth, and three accumulations. CD curves for peptide, peptide/drug, peptide/liposome and peptide/liposome/drug samples were corrected with a blank buffer solution. Titration with suramin in the presence and in the absence of liposomes was performed in duplicate with use of CD buffer and as a single experiment in PBS. To estimate CM15 secondary structure content under various conditions, the software provided by the BeStSel (Beta Structure Selection) website (http://bestsel.elte.hu)[30] was used. Data points are given as means ± standard errors of means (SEMs).

Dynamic light scattering (DLS): Mean hydrodynamic diameter (D_h) and polydispersity were measured at 20 °C with a W130i dynamic light scattering device (DLS, Avid Nano, Ltd., High Wycombe, UK) with a diode laser (660 nm) and a photodiode detector. Low-volume disposable cuvettes with 1 cm path length (UVette, Eppendorf Austria, GmbH) were used. Samples containing peptide (20 μM) and various amounts of drug and liposomes were measured in a final volume of 80 μL in PBS. The time-dependent autocorrelation functions were measured for 10 s, this was repeated ten times, and the average distributions were reported. The analysis of the measurement data was performed with the iSize 3.0 software, supplied with the device.

Attenuated total reflection (ATR) FTIR: FTIR spectroscopic measurements were conducted with a Varian 2000 FTIR Scimitar spectrometer (Varian, Inc, US) fitted with a liquid-nitrogen-cooled mercury/cadmium/telluride (MCT) detector and a "Golden Gate" single-reflection diamond ATR accessory (Specac, Ltd, UK). The sample (5 μL) was mounted onto the diamond ATR surface, and the spectra were collected (2 cm^{-1} resolution and 64 scans) from dry films (after slow evaporation of the buffer solvent under ambient conditions). Prior to spectral evaluation, ATR correction was performed and the corrected spectra were smoothed with use of the Savitzky–Golay algorithm (polynomial degree = 2, number of points = 17) and the GRAMS/32 (Galactic, Inc., USA) software package.

Fluorescence spectroscopy: Spectra were recorded with a Jobin Yvon Fluoromax-3 spectrofluorimeter (3 and 5 nm excitation and emission slits, respectively), at 25 °C in PBS. To test peptide interaction, the tryptophan fluorophore of CM15 was excited at 295 nm and emission was monitored from 310 to 400 nm. Binding assays were carried out with CM15 at 1 μM in the presence and absence of liposomes being titrated with increasing amounts of suramin up to 50 μM. To correct for spectral contribution of the liposomes and suramin, appropriate blank spectra (recorded for solutions containing no fluorophore but lipid and drug at the same concentration) were subtracted. Peptide titrations were performed in duplicate; data presented are means ± SEMs.

Transmission electron microscopy (TEM): For direct visualisation of the structure and morphology of the sample, TEM images were obtained with a Morgagni 268D instrument (FEI, The Netherlands). A droplet (2 μL) of the sample prepared in PBS was pipetted onto a 200 mesh copper grid with a support film made of formvar. Excess liquid was removed after a 20 s contact time. Phosphotungstic acid (5%) was added immediately as contrast material; then, after a contact time of 10 min, excess liquid was again removed and the sample was left to air-dry.

Antibacterial test, cytotoxicity and haemolytic assay: The antibacterial effect of CM15 in the presence or in the absence of suramin was measured with *E. coli* strain DSM 1103. Bacterial lyophilisate was resuspended in Bouillon broth and cultured in a blood agar plate for 24 h. To test peptide efficacy, 0.5 McFarland standard was diluted 50 times, and bacterial suspension (100 μL) was then plated on a 96-well U-bottomed plate. Lysogeny broth (LB) was used as culture medium. CM15 solutions alone or together with suramin were added to the wells in a final concentration of 40, 20, 10, and 5 μM for each compound. Plates were read after 24 h incubation. All samples were measured in quadruplet; data are means ± SEMs.

Cytotoxic effects of CM15 were measured with the MonoMac6 human monocytic cell line (DSMZ, ACC 124), widely used and accepted as model cells for assays of cytotoxicity, membrane damage and cellular uptake of compounds such as peptides or drugs.[31] Prior to the treatment, cells were cultured in serum-free RPMI medium and plated (15000 cells, 100 μL/well) in a flat-bottomed 96-well plate. CM15 was dissolved in serum-free medium at a final concentration of 200 μM. Suramin was added to the peptide solution at 1:1 or 1:2 molar ratio. Cells were treated with serial dilution of CM15 or CM15/suramin mixtures over the concentration range of 0.8–100 μM in triplicate. Cells were incubated with the compounds for 1.5 h, and cell viability was then tested by use of the (4,5-dimethylthiazol-2-yl)-2,5-diphenyltetrazolium bromide (MTT) assay.[32] Briefly, MTT solution (45 μL) was added to each well (2 mg mL^{-1}, dissolved in serum-free medium). After 3.5 h incubation, plates were centrifuged at 430 *g* for 5 min, and the supernatant was carefully aspirated with a G30 needle. The precipitated purple crystals were dissolved in DMSO (100 μL), and after 10 min agitation the absorbance was determined at 540 and 620 nm with use of an ELISA plate reader (iEMS Reader, Labsystems). Cytotoxicity, expressed as a percentage as a function of peptide concentration, was plotted, and IC_{50} values were determined. Data are means ± SEMs ($n = 3$).

For haemolytic activity assay, peripheral blood from a healthy volunteer (purchased from the Hungarian National Blood Transfusion Service, Budapest, Hungary) was collected in vacuum tubes containing sodium citrate as anticoagulant (Vacuette, 9NC). Tubes were centrifuged (430 *g*, 5 min) and the pellet was washed twice with PBS. PBS was added to the pellet to yield a final RBC suspension (4%, *v/v*). Stock solutions of the compounds were diluted in PBS and twofold serial dilution series were prepared (final concentrations 1.6–200 μM). RBC suspension (100 μL/well) was placed in a 96-well U-bottomed cell culture plate and mixed with peptide solution (100 μL). The plates were incubated for 1.5 h at 37 °C. After centrifugation (430 *g*, 5 min), the supernatant (50 μL) was transferred to a flat-bottomed microtiter plate and absorbance was measured at 414/450 nm with an ELISA plate reader. Percentage haemolysis was plotted against peptide concentration, and HC_{50} values were determined. Data are means ± SEMs ($n = 3$).

To analyse statistical significance (p), the Student t-test was performed by using GraphPad Prism.

Acknowledgements

This work was supported through grants provided by the Momentum Program (LP2016-2), the National Competitiveness and Excellence Program (NVKP_16-1-2016-0007) and GINOP (BIONANO_GINOP-2.3.2-15-2016-00017). We also thank the National

Research Development and Innovation Office, Hungary (grants OTKA 104275, 115431, 124077) and additionally are grateful for grants (VEKOP-2.3.3-15-2017-00020, VEKOP-2.3.2-16-2017-00014) from the European Union and the State of Hungary, co-financed by the European Regional Development Fund. K.H. was supported by the János Bolyai Research Scholarship of the Hungarian Academy of Sciences. Sz.B. thanks the ELTE Institutional Excellence Program (783-3/2018/FEKUTSRAT) supported by the Hungarian Ministry of Human Capacities.

Conflict of Interest

The authors declare no conflict of interest.

Keywords: antimicrobial peptides · circular dichroism · folding · IR spectroscopy · suramin

[1] a) D. Dominey-Howes, B. Bajorek, C. A. Michael, B. Betteridge, J. Iredell, M. Labbate, *Front. Microbiol.* **2015**, *6*, 927; b) Y. Li, Q. Xiang, Q. Zhang, Y. Huang, Z. Su, *Peptides* **2012**, *37*, 207 – 215; c) K. A. Brogden, *Nat. Rev. Microbiol.* **2005**, *3*, 238; d) A. Hollmann, M. Martinez, P. Maturana, L. C. Semorile, P. C. Maffia, *Front. Chem.* **2018**, *6*, 204.

[2] a) Y. J. Gordon, E. G. Romanowski, A. M. McDermott, *Curr. Eye Res.* **2005**, *30*, 505 – 515; b) R. E. W. Hancock, H.-G. Sahl, *Nat. Biotechnol.* **2006**, *24*, 1551; c) M. N. Melo, R. Ferre, M. A. R. B. Castanho, *Nat. Rev. Microbiol.* **2009**, *7*, 245; d) K. N. Alfieri, A. R. Vienneau, C. H. Londergan, *Biochemistry* **2011**, *50*, 11097 – 11108.

[3] A. Milani, M. Benedusi, M. Aquila, G. Rispoli, *Molecules* **2009**, *14*, 5179 – 5188.

[4] a) T. Ganz, *Nat. Rev. Immunol.* **2003**, *3*, 710; b) R. Hancock, A. Patrzykat, *Curr. Drug Targ. Infect. Disord.* **2002**, *2*, 79 – 83; c) P. Kumar, J. Kizhakkedathu, S. K. Straus, *Biomolecules* **2018**, *8*, 4.

[5] a) F. Zsila, S. Bosze, K. Horvati, I. C. Szigyarto, T. Beke-Somfai, *RSC Adv.* **2017**, *7*, 41091 – 41097; b) K. E. S. Locock, *Aust. J. Chem.* **2016**, *69*, 717 – 724; c) S. Pistolesi, R. Pogni, J. B. Feix, *Biophys. J.* **2007**, *93*, 1651 – 1660.

[6] E. H. Mattar, H. A. Almehdar, H. A. Yacoub, V. N. Uversky, E. M. Redwan, *Cytokine Growth Factor Rev.* **2016**, *28*, 95 – 111.

[7] a) S. E. Blondelle, B. Forood, R. A. Houghten, E. Pérez-Payá, *Biopolymers* **1997**, *42*, 489 – 498; b) H. J. Dyson, P. E. Wright, *Nat. Rev. Mol. Cell Biol.* **2005**, *6*, 197.

[8] a) M.-A. Sani, F. Separovic, *Acc. Chem. Res.* **2016**, *49*, 1130 – 1138; b) P. Maturana, M. Martinez, M. E. Noguera, N. Santos, E. A. Disalvo, L. Semorile, P. C. Maffia, A. Hollmann, *Colloids Surf. B* **2017**, *153*, 152 – 159; c) T. Shireen, A. Basu, M. Sarkar, K. Mukhopadhyay, *Biophys. Chem.* **2015**, *196*, 33 – 39.

[9] F. Zsila, T. Juhász, S. Bősze, K. Horváti, T. Beke-Somfai, *Chirality* **2018**, *30*, 195 – 205.

[10] T. Juhász, J. Mihály, G. Kohut, C. Németh, K. Liliom, T. Beke-Somfai, *Sci. Rep.* **2018**, *8*, 14499.

[11] V. Fourneau, J. Tréfouel, J. Vallée, *Ann. Inst. Pasteur* **1924**, *38*, 81 – 114.

[12] a) L. Henß, S. Beck, T. Weidner, N. Biedenkopf, K. Sliva, C. Weber, S. Becker, B. S. Schnierle, *Virol. J.* **2016**, *13*, 149; b) J. E. Allen, O. Adjei, O. Bain, A. Hoerauf, W. H. Hoffmann, B. L. Makepeace, H. Schulz-Key, V. N. Tanya, A. J. Trees, S. Wanji, D. W. Taylor, *PLoS Neglected Trop. Dis.* **2008**, *2*, e217; c) C. P. Chijioke, R. E. Umeh, A. U. Mbah, P. Nwonu, L. L. Fleckenstein, P. O. Okonkwo, *Eur. J. Clin. Pharmacol.* **1998**, *54*, 249 – 251; d) B. Thylefors, *Bull. World Health Org.* **1978**, *56*, 63 – 73.

[13] A. J. Nok, *Parasitol. Res.* **2003**, *90*, 71 – 79.

[14] a) M. R. Mirza, E. Jakobsen, P. Pfeiffer, B. Lindebjerg-Clasen, J. Bergh, C. Rose, *Acta Oncolog.* **1997**, *36*, 171 – 174; b) M. A. Eisenberger, L. M. Reyno, D. I. Jodrell, V. J. Sinibaldi, K. H. Tkaczuk, R. Sridhara, E. G. Zuhowski, M. H. Lowitt, S. C. Jacobs, M. J. Egorin, *J. Natl. Cancer Inst.* **1993**, *85*, 611 – 621; c) R. Dreicer, D. C. Smith, R. D. Williams, W. A. See, *Invest. New Drugs* **1999**, *17*, 183 – 186; d) G. H. Salvador, T. R. Dreyer, A. A. Gomes, W. L. Cavalcante, J. I. Dos Santos, C. A. Gandin, M. de Oliveira Neto, M. Gallacci, M. R. Fontes, *Sci. Rep.* **2018**, *8*, 10317.

[15] R. Gautier, D. Douguet, B. Antonny, G. Drin, *Bioinformatics* **2008**, *24*, 2101 – 2102.

[16] R. W. Woody, *Instrum. Anal. Intrinsically Disord. Proteins* **2010**, 303 – 321.

[17] B. Nordén, A. Rodger, T. Dafforn, *Linear Dichroism and Circular Dichroism*, The Royal Society of Chemistry, **2010**.

[18] K. Matsuzaki, *Biochim. Biophys. Acta Biomembranes* **1999**, *1462*, 1 – 10.

[19] D. Ganguly, G. Chamilos, R. Lande, J. Gregorio, S. Meller, V. Facchinetti, B. Homey, F. J. Barrat, T. Zal, M. Gilliet, *J. Exp. Med.* **2009**, *206*, 1983 – 1994.

[20] a) A. Ghisaidoobe, S. Chung, *Int. J. Mol. Sci.* **2014**, *15*, 22518 – 22538; b) J. R. Tusell, P. R. Callis, *Biophys. J.* **2011**, *100*, 174a.

[21] S. Gilch, K. F. Winklhofer, M. H. Groschup, M. Nunziante, R. Lucassen, C. Spielhaupter, W. Muranyi, D. Riesner, J. Tatzelt, H. M. Schätzl, *EMBO J.* **2001**, *20*, 3957 – 3966.

[22] G. Kohut, A. Sieradzan, F. Zsila, T. Juhász, S. Bősze, A. Liwo, S. A. Samsonov, T. Beke-Somfai, *Phys. Chem. Chem. Phys.* **2019**, DOI: https://dx.doi.org/10.1039/C9CP00471H.

[23] a) S. L. Fleck, B. Birdsall, J. Babon, A. R. Dluzewski, S. R. Martin, W. D. Morgan, E. Angov, C. A. Kettleborough, J. Feeney, M. J. Blackman, A. A. Holder, *J. Biol. Chem.* **2003**, *278*, 47670 – 47677; b) C. R. Middaugh, H. Mach, C. J. Burke, D. B. Volkin, J. M. Dabora, P. K. Tsai, M. W. Bruner, J. A. Ryan, K. E. Marfia, *Biochemistry* **1992**, *31*, 9016 – 9024; c) Q. Wu, J. Wang, L. Zhang, A. Hong, J. Ren, *Angew. Chem. Int. Ed.* **2005**, *44*, 4048 – 4052; *Angew. Chem.* **2005**, *117*, 4116 – 4120; d) Y. L. Zhang, Y. F. Keng, Y. Zhao, L. Wu, Z. Y. Zhang, *J. Biol. Chem.* **1998**, *273*, 12281 – 12287.

[24] a) K. Bhargava, J. B. Feix, *Biophy. J.* **2004**, *86*, 329 – 336; b) H. Sato, J. B. Feix, *Biochim. Biophys. Acta Biomembranes* **2006**, *1758*, 1245 – 1256; c) M. Sharon, Z. Oren, Y. Shai, J. Anglister, *Biochemistry* **1999**, *38*, 15305 – 15316; d) M. Bastos, G. Bai, P. Gomes, D. Andreu, E. Goormaghtigh, M. Prieto, *Biophys. J.* **2008**, *94*, 2128 – 2141.

[25] J. W. Brauner, R. Mendelsohn, F. G. Prendergast, *Biochemistry* **1987**, *26*, 8151 – 8158.

[26] a) N. Lehmann, G. K. Aradhyam, K. Fahmy, *Biophys. J.* **2002**, *82*, 793 – 802; b) M. Y. Skripkin, P. Lindqvist-Reis, A. Abbasi, J. Mink, I. Persson, M. Sandström, *Dalton Trans.* **2004**, 4038 – 4049.

[27] T. Polenova, T. Iwashita, A. G. Palmer, 3rd, A. E. McDermott, *Biochemistry* **1997**, *36*, 14202 – 14217.

[28] a) P. Juvvadi, S. Vunnam, E. L. Merrifield, H. G. Boman, R. Merrifield, *J. Pept. Sci.* **1996**, *2*, 223 – 232; b) H. Sato, J. B. Feix, *Antimicrob. Agents Chemother.* **2008**, *52*, 4463 – 4465.

[29] C. J. Bowden, W. D. Figg, N. A. Dawson, O. Sartor, R. J. Bitton, M. S. Weinberger, D. Headlee, E. Reed, C. E. Myers, M. R. Cooper, *Cancer Chemother. Pharmacol.* **1996**, *39*, 1 – 8.

[30] A. Micsonai, F. Wien, L. Kernya, Y.-H. Lee, Y. Goto, M. Réfrégiers, J. Kardos, *Proc. Natl. Acad. Sci. USA* **2015**, *112*, E3095 – E3103.

[31] a) H. L. Ziegler-Heitbroc, E. Thiel, A. Futterer, V. Herzog, A. Wirtz, G. Riethmüller, *Int. J. Cancer* **1988**, *41*, 456 – 461; b) É. Kiss, G. Gyulai, E. Pári, K. Horváti, S. Bősze, *Amino Acids* **2018**, *50*, 1557 – 1571; c) K. Horváti, B. Bacsa, T. Mlinkó, N. Szabó, F. Hudecz, F. Zsila, S. Bősze, *Amino Acids* **2017**, *49*, 1053 – 1067.

[32] a) Y. Liu, D. A. Peterson, H. Kimura, D. Schubert, *J. Neurochem.* **1997**, *69*, 581 – 593; b) T. Mosmann, *J. Immunol. Methods* **1983**, *65*, 55 – 63; c) E. C. Slater, *Ned. Tijdschr. Geneeskd.* **1963**, *107*, 1543 – 1544.

Manuscript received: December 21, 2018

Accepted manuscript online: February 5, 2019

Version of record online: May 20, 2019

